EUV OBSERVATIONS OF QUIESCENT PROMINENCES FROM SKYLAB

O. KJELDSETH MOE
Institute of Theoretical Astrophysics, University of Oslo, Oslo, Norway

J. W. COOK and S. A. MANGO
E. O. Hulburt Center for Space Research, Naval Research Laboratory, Washington, D.C., U.S.A.

(Received 31 October, 1978)

Abstract. We report measurements of line intensities and line widths for three quiescent prominences observed with the Naval Research Laboratory slit spectrograph on ATM/Skylab. The wavelengths of the observed lines cover the range 1175 Å to 1960 Å. The measured intensities have been calibrated to within approximately a factor 2 and are average intensities over a 2 arc sec by 60 arc sec slit. We derive nonthermal velocities from the measured line widths. The nonthermal velocity is found to increase with temperature in the prominence transition zone. Electron densities and pressures are derived from density sensitive line ratios. Electron pressures for two of the prominences are found to lie in the range 0.04–0.08 dyn cm^{-2}, while values for the third and most intense and active of the three prominences are in the range 0.07–0.22 dyn cm^{-2}.

1. Introduction

The EUV spectral region contains a number of emission lines formed at temperatures ranging from the photospheric to the coronal. Together with radio observations, EUV measurements allow derivation of physical parameters, such as pressure and temperature structure, through the transition zone.

Solar EUV intensities can only be measured by instruments flown on rockets or satellites. Rocket observations of prominences were made by the consortium UV spectrograph flown during the solar eclipse of March 7, 1970 (Speer *et al.*, 1970). Orrall and Speer (1974) reported on two prominences observed by this instrument and further analysis of the material was presented by Yang *et al.* (1975).

Because of their relative faintness, longer integration times are required for prominence observations than for the solar disk to obtain intensities for a similar number of lines. Observations from satellites are thus necessary to record any but the strongest EUV emission lines. Satellite observations of prominences were carried out by OSO-IV and OSO-VI and results have been reported by Withbroe (1971) and by Noyes *et al.* (1972).

During Skylab a large number of prominences of all types were observed in wavelengths ranging from X-rays to visual coronagraphic observations of transients from eruptive prominences. EUV measurements have been reported by Schmahl *et al.* (1974) and by Orrall and Schmahl (1976) from the Harvard College Observatory instrument. Feldman and Doschek (1977) reported observations from an unspecified prominence using the Naval Research Laboratory S082B instrument.

Solar Physics **61** (1979) 319–334. 0038-0938/79/0612-0319 $02.40.

This paper presents additional measurements from the S082B data. Three prominences have been included with several pointings in each prominence. The wavelength range 1175 Å to 1930 Å contains several density sensitive line pairs. The structure of the transition zone 30 000 K to 200 000 K may in principle be derived from the intensities of resonance lines in this wavelength range. However, the transition zone structure also depends on the geometrical structure of the prominence and on the direction of the magnetic field. Details concerning both these factors are largely undetermined. Discussion of various prominence models is referred to a second paper (Paper II) where the temperature structure and energy balance of the prominence transition zone are discussed. Paper II will derive the temperature structure assuming various geometries of the prominence and magnetic field.

2. Instrument and Observations

2.1. Telescope and spectrograph

The observations were made with the Naval Research Laboratory S082B slit spectrograph aboard ATM/Skylab. The instrument has been described in detail by Bartoe *et al.* (1977). A telescope mirror of 1 m focal length formed a solar image of diameter 9.3 mm on the entrance slit of the spectrograph, with an angular resolution of approximately 1 arc sec. The size of the spectrograph slit was 10 μm by 300 μm corresponding to 2 arc sec by 60 arc sec on the Sun. Because of the construction of the spectrograph, with crossed dispersion of the predisperser and main gratings, there is no resolution along the slit. The slit size therefore determines the angular resolution of the observations. Pointing stability was better than ±2 arc sec.

The spectrograph was a double dispersion, normal incidence grating spectrograph. Observations could be made in both first and second order of the main grating. The wavelength ranges covered were 1940–3940 Å and 970–1960 Å, respectively. When observing in the second order on the solar disc the spectra were contaminated by stray light in the spectrograph from the first order wavelength region (see Bartoe *et al.*, 1977). However, in prominences, as in all near- and off-limb observation, the continuum between 2000 Å and 4000 Å is too weak to result in any noticeable contamination. Indeed there is no trace of any stray light from the first order in our observations. Neither is there any stray light in the telescope from the disc at the distance from the limb where the prominence spectra were observed.

The observations reported are all of emission lines from the second order wavelength region. The linear dispersion of the spectrograph was approximately 4.16 Å mm^{-1} and the spectral resolution 0.06 Å.

2.2. Selection of observations

Several quiescent prominences were observed with S082B during the Skylab missions. We have selected data from three prominences, all from the last manned

mission. The prominences are P37 observed on December 1, 1973; P39 on December 5, 1973, and P76 observed on January 12, 1974. The three prominences were located in the northern hemisphere at latitudes 35°, 15°, and 35°, respectively.

Table I gives data for the selected exposures. The first column identifies the prominence and gives the angle, ϕ, between the line of sight and the axis along the prominence. The angle is estimated from the orientation of the corresponding $H\alpha$ filament to the meridian measured at meridian passage one week before or after the observations. A possible change in this angle in the intervening time, caused by differential rotation, has been disregarded.

TABLE I

Data for the exposures used for measurements of the prominence EUV intensities

Prominence (orientation)	ATM plate no.	UT time for start of exposure (day : hr : min)	Exposure-time (s)	Altitude of slit (km)	Inclination of slit	Slit fill-factor
P37	3B-006-8	$335^d:22^h:08^m$	960	24 000	90	1.0
($\phi = 50°$)	3B-007-2	:22 :40	366	—	—	—
	3B-024-7	$339^d:14^h:38^m$	428	13 000	92	0.8
	3B-025-1	:17 :48	600	10 000	90	0.7
P39	3B-025-2	:18 :07	599	—	—	0.4(?)
($\phi = 120°$)	3B-025-3	:18 :18	551	—	—	
	3B-025-4	:20 :48	359	17 000	96	0.6
	3B-025-5	:20 :54	719	—	—	—
P76	3B-163-2	$012^d:19^h:51^m$	839	21 000	28	
($\phi = 45°$)	3B-163-6	:21 :16	840	20 000	—	
	3B-164-5	:22 :51	840	27 000	—	

The second and third columns in Table I give the S082B platenumbers and the times for the start of the exposure. The exposure times are given in the fourth column. For all three prominences we have chosen to present data from exposures in the range 360 to 960 s. This gives the most complete record of line intensities for all prominence emission lines observable with the S082B instrument and film using exposure times up to 1000 s. Any longer exposures do not exist.

However, because of the long exposure times some of the strongest lines, even in the relatively faint prominence spectrum, may be overexposed. Owing to the limited dynamic range of the film, intensities of both strong and weak lines cannot be recorded on a single exposure. Shorter exposures of the prominence spectrum exist, particularly in the case of P76, and it might be possible to measure the intensities of the strongest lines from these exposures. However, there are possibly intrinsic changes in the prominence intensities with time. We have therefore decided to present only the exposures giving the most complete set of measured intensities even at the cost of leaving out intensity values for some of the stronger lines at some pointings. Most of the strong lines have been measured in several of the exposures.

The only noticeable exception is the $L\alpha$ line of hydrogen which has been entirely left out of the list of line intensities.

2.3. Observing procedures and pointing of the slit

Using the on-board Hα telescope (Markey and Austin, 1977) the Skylab astronauts placed the S082B slit along what appeared to be regions of relatively uniform prominence Hα emission. A single exposure or series of exposures was then taken. Detailed information on the slit positions is given in the three last columns of Table I. Given are the altitudes in km of the mid-point of the slit above the limb, the angle of inclination of the slit to the 'solar vertical' and estimates of the slit fill factor.

The slit positions relative to the prominence material are also documented in Figure 1 for prominences P37 and P39. Figure 1 is copied from pointing exposures taken with the Hα 1 telescope on Skylab (Markey and Austin, 1977). Unfortunately, P76 was too weak in Hα to register on the pointing pictures. When comparing the slit altitudes in Figure 1 with the numbers in Table I one should take into account that the pointing pictures are reproduced from strongly overexposed Hα images. The limb in Figure 1 corresponds to the tops of the spicules, 5–6 arc sec above the limb referred to in Table I.

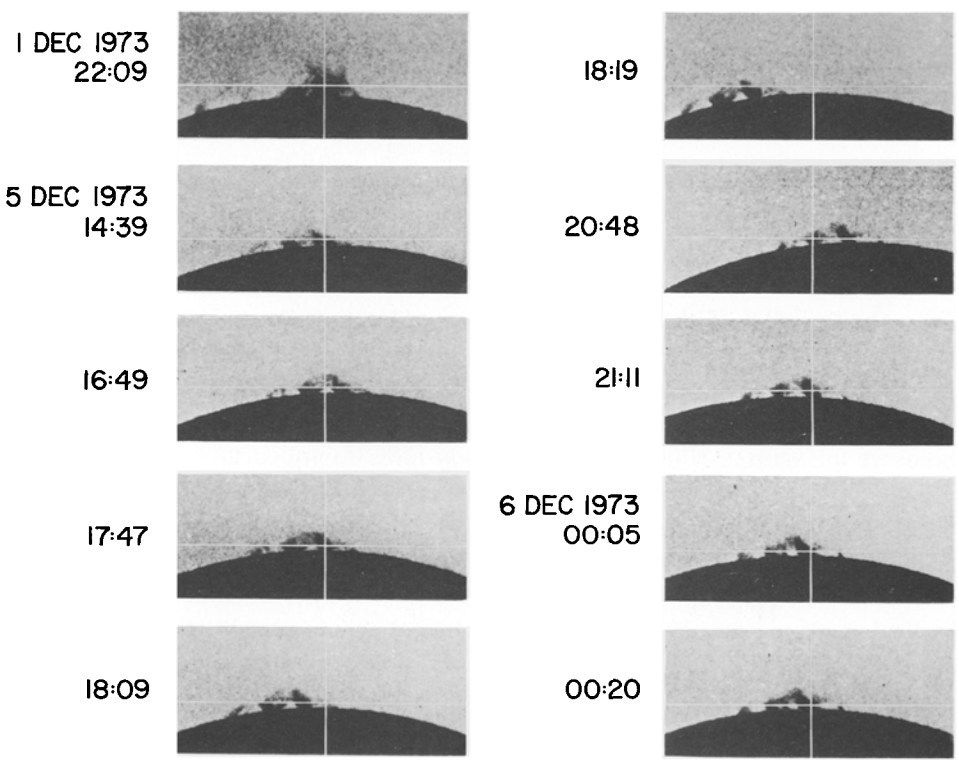

Fig. 1. The pointing of the S082B slit in prominences P37 and P39.

The slit fill factors are estimated from the Hα 1 pictures. The estimates are rather uncertain. In all cases for which a fill factor is given, the entire slit is filled with Hα emitting gas. However, the intensity of the Hα emissions varies along the slit. A fill factor value of 1.0 for P37 means that the slit is entirely filled with strongly emitting gas. For exposure 3B-025-1, where a fill factor of 0.7 is listed, about one half of the slit is filled with strong emission in Hα. The remaining half of the slit contains weaker emitting gas.

For P76 the slit positions and orientations have been estimated from the pointing reference system data and fill factors are obviously lacking.

2.4. Intensity calibration and accuracy of photometry

The spectra were recorded on Eastman Kodak Type 104 emulsion. Absolute intensity calibration of the instrument and film has been carried out by Kjeldseth Moe and Nicolas (1977). Calibration was accomplished by comparing the intensities from calibration rocket flights (CALROC) on the second and third Skylab missions with relative intensities of the same solar areas observed nearly simultaneously by S082B. The sensitivity of the CALROC instruments were accurately determined against a deuterium lamp and an argon arc measured at the National Bureau of Standards. Combining the errors in the calibration of the standard sources, the rocket calibrations, and the transfer of the calibration to the Skylab S082B instrument, leads to an estimated accuracy of the measured absolute intensities of ±50%. Relative intensities of lines, particularly lines close together in wavelength, may be as good as 20%. These estimates, however, are valid only for film densities on the linear portion of the film characteristic curve. For densities in the toe or shoulder of the curve the measured values are considerably more uncertain.

The film characteristic curves were constructed from the flight exposures. The method consisted of comparing film densities above fog level at exactly the same wavelengths on exposures taken at the same pointing, but with different exposure times. Detailed descriptions of the method and results are given in papers by Kjeldseth Moe and Nicolas (1977) and Kjeldseth Moe and Milone (1978). These papers also describe the procedures of scanning the plates and Fourier smoothing to remove noise in the data.

In addition to the data reduction procedures described by these authors, two additional points need to be made for the prominence observations.

Firstly, the exposure series used to determine the film characteristic curves were not part of the prominence observations. For pointings in the prominences, series of exposures taken with different exposure times at the same pointing cover only the exposure times 10, 40, and 160 s. Particularly the two shorter exposures show in prominences only a few spectral features. This precluded construction of reliable characteristic curves at a sufficient number of wavelengths through the second order spectral range. The characteristic curves thus had to be determined from or checked against observations taken on the disc, but fairly close to the limb to avoid stray light contamination. Exposure times for these limb spectra were in the range 1 to 100 s.

Care was taken to use disc observations belonging to the same film and development batches as the prominence observations.

A second concern is the possibility of reciprocity failure of the type 104 emulsion. So far one has assumed the film to be perfectly reciprocal. Deviations from reciprocity would lead to systematic errors in both the constrast and absolute scale of the derived characteristic curves. As long as intensities are measured from spectra with exposure times in the same range as those used to construct the characteristic curves the errors are relatively small and not necessarily systematic.

However, the prominence intensities are derived from exposures 3 to 10 times longer than those used for the characteristic curves. Quantitative information on the reciprocity properties of the type 104 emulsion is scarce. Van Hoosier (1978) reports that this emulsion is very nearly reciprocal in the exposure time range 1–100 s for exposures made at normal atmospheric pressures. For exposures made in vacuum the range of reciprocity for the film is expected to increase.

In conclusion one may estimate rms errors in the absolute intensity determination to ±50%. A systematic error because of reciprocity failure is possible, but will not exceed a factor 2 (Van Hoosier, 1978) and is likely to be lower than that.

3. Results

3.1. Emission line intensities and widths

In Table II we present the measured intensities and line widths of 95 emission lines observable in our exposures. The intensity values are given in ergs cm^{-2} s^{-1} sr^{-1} and represent total integrated line intensities. The widths are in mÅ and are full widths at half maximum intensity, FWHM. The effect of slit fill factors different from 1.0 has not been taken into account in Table II. The values represent intensities averaged over the full length of the slit. As discussed in Section 2.2 intensity values are not given for lines that are over-exposed in our selected exposure. Furthermore, no continuum is observable for wavelengths below 1960 Å.

We note that the intensities for exposure 3B-025-3 have been left out of Table II. Looking at the Hα pointing picture in Figure 2 we see that this exposure was taken at a position where the prominence emission in Hα was very faint and of small extent. This is reflected in the UV spectra which has only a few of the strongest UV-lines present.

With the exception of Lα the 95 lines represent all the features appearing on the plates. The original spectra have been examined by eye to verify the presence of the weakest features. Except for six lines, the O IV line at 1399.77 Å, the S IV line at 1406.00 Å, the Si VIII line at 1445.75 Å and the three unidentified features at 1298.97 Å, 1446.41 Å, and 1749.60 Å, all the lines have measurable intensities on several exposures. Weak lines with intensities marked as unmeasurable (symbol *g* in Table II) have peak intensities falling below the threshold for reliable photometry. This threshold has been set at a level corresponding to a film density 0.05 above fog.

The wavelengths of the lines have been taken from Kelly and Palumbo (1973). Exceptions are the unidentified or blended lines where solar wavelengths have been used, and the Si VIII line where the wavelength was taken from the list of coronal lines by Sandlin *et al.* (1977).

The integrated intensities of Table II were derived from the intensity at line center and the measured width, assuming the line profile to be gaussian. The assumption of a gaussian profile appears to be a good one for most of the lines. The few exceptions are marked with *f* in Table II. For these asymmetric lines the intensity values are reached by actual integration across the line profiles.

3.2. Estimated errors for line widths and intensities

In addition to the calibration errors discussed in Section 2.4, the intensities in Table II are also subject to uncertainties because of errors in the measured widths. For lines where both the peak intensity and the half intensity level fall on the reliable portion of the film characteristic curve, the widths of the lines may be determined to within 10–15 mÅ. For most of the lines, with exception of the narrowest, this amounts to an accuracy of 10% or better.

Some of the lines are too weak to allow measurements of the half intensity width. The level of half maximum intensity falls below the sensitivity threshold for reliable photometry. For these cases the FWHM may be estimated from a point higher on the profile, again assuming gaussian line profile. This method has been used only for those lines where the half intensity level is very close to the threshold. The lines are marked *d* in Table II. Also for weak lines the widths may be estimated from the values for stronger lines of the same multiplet or ion (marked *c* or *j* in Table II).

One will notice some peculiar values in the list of line widths. For example the width of the O I line of 1355.60 Å is measured as 54 mÅ on plate 3B-025-4, which is less than the instrumental width. Also other measured widths of this line are rather close to the instrumental limit. The fact that line widths narrower than the instrumental width may occur is caused by noise in the film. Aggregation of film grains may on occasion lead to values of maximum film density in the line-center that are too high. Thus the measured half intensity level will lie above the actual one causing an underestimation of the line width.

Another set of peculiar values of line widths are the measured widths of the O V line at 1371.29 Å in P76. The values, 120 mÅ and 125 mÅ, are less than the thermal width and fall below the width expected from the measurement of the O V line at 1218.36 Å with 30 mÅ to 70 mÅ. In this case the reason must be the very low peak intensity of these lines, rendering the measured widths particularly uncertain.

Thus the uncertainty in the measured widths will not add appreciably to the error in the absolute intensity for lines above a certain intensity level. For these lines the calibration is the dominating source of error. However, for line intensities below approximately 10 ergs cm^{-2} s^{-1} sr^{-1} the error in the measured widths becomes increasingly important. For the weaker lines this may be the most important source of error for the intensity determination.

TABLE II

Line intensities and widths for the EUV emission lines 1175 Å to 1930 Å observed in three quiescent prominences

Wavelength[a] Å	Identification	P37 – Dec. 1, 1973						P39 – Dec. 5, 1973								P76 – Jan. 12, 1974					
		3B-006-8		3B-007-2		3B-024-7		3B-025-1		3B-025-2		3B-025-4		3B-025-5		3B-163-2		3B-163-6		3B-164-5	
		I	FWHM (mÅ)	I	FWHM (mÅ)	I	FWHM (mÅ)	I	FWHM (mÅ)	I	FWHM (mÅ)	I	FWHM (mÅ)	I	FWHM (mÅ)	I	FWHM (mÅ)	I	FWHM (mÅ)	I	FWHJM (mÅ)
1175.711	C III(4)	24.1	197	24.1	200[c]	—	—[e]	23.4	120	—	—[g]	42.4	154[d]	41.7	177	12.2	125	16.7	145	13.5	125
1206.533	Si III(11)	68.5	217	98.1	219	30.3	105	27.1	97	26.4	117	77.4	228	52.3	203	38.8	145	47.8	167	39.2	140
1218.360	O V	20.2	205	20.5	200	21.7	190	20.6	197	12.4	187	37.0	211	26.7	230	16.5	155	19.4	170	15.2	140
1238.821	N V(1)	29.6	211	34.1	182	26.2	160	26.3	173	14.6	170	44.5	190	34.6	201	28.3	160	28.3	180	21.5	150
1242.000	Fe XII	—	—[e]	—	—[e]	20.1	290	17.1	250	18.7	280	26.0	300[d]	17.2	250	—	—[e]	—	—[e]	—	—[e]
1242.804	N V(1)	17.0	181	15.7	168	14.4	146	14.1	152	8.3	154	29.2	190	23.8	191	15.5	130	14.3	162	12.2	135
1259.530	S II(1)	3.0	120[d]	—	—[e]	—	—[e]	—	—[g]	—	—[e]	—	—[e]	4.3	88[d]	—	—[e]	—	—[e]	—	—[e]
1260.421	Si II(4)	8.8	148	7.5	148[c]	—	—[g]	6.4	106[d]	6.5	110	14.0	185[c]	9.2	129	2.9	110[d]	3.0	112[c]	3.0	100[d]
1264.737	Si II(4)	24.0	162	23.2	152	13.9	118	12.5	113	10.8	105	25.6	185	18.1	153	8.6	125	9.3	120	9.7	110
1265.001	Si II(4)	8.5	155[c]	7.2	152[c]	—	—[g]	5.8	110[c]	5.1	107[c]	11.4	185[c]	9.1	141[c]	2.7	125[c]	2.9	120[c]	2.8	90
1298.970	Unident.	—	—[e]	—	—[e]	—	—[e]	—	—[e]	—	—[e]	—	—[e]	—	—[e]	—	—[e]	2.4	125[d]	—	—[g]
1302.169	O I(2)	66.7	125	78.7	165	43.1	115	43.5	101	23.7	102	54.0	102	40.8	106	30.0	100	21.2	100	31.0	90
1304.372	Si II(3)	9.0	133	6.7	100[d]	10.7	125[d]	6.7	75	4.4	70	9.1	104[c]	7.2	88	2.8	90[d]	2.5	95[c]	3.3	70[d]
1304.858	O I(2)	71.2	163	75.2	154	45.7	103	43.1	93	22.0	94	52.4	94	40.3	100	25.2	90	20.0	90	26.4	90
1306.029	O I(2)	53.5	130	62.8	136	41.3	95	39.1	88	19.3	74	49.5	94	35.7	90	19.1	90	12.1	90	20.0	75
1309.277	Si II(3)	11.9	138	10.5	128	11.2	125[d]	8.9	84	5.9	86[d]	11.8	104[d]	10.7	118	3.6	90	9.7	95	5.0	85
1334.532	C II(1)	—	—[h]	165.0	190	74.6	125	65.5	113	48.0	120	111.2	125	73.4	150	—	—[h]	—	—[h]	—	—[h]
1335.708[b]	C II(1)	—	—[h]	235.0	—[f]	118.0	133	93.5	138[h]	68.9	150	156.0	163	98.8	177[h]	—	—[h]	—	—[h]	—	—[h]
1355.598	O I(1)	11.0	91	11.2	77	12.3	68	10.0	63	3.5	68[d]	15.7	54	12.0	62	—	—[g]	—	—[e]	2.3	70[d]
1371.292	O V(7)	3.7	134[d]	—	—	—	—[e]	—	—[e]	—	—[e]	—	—[e]	7.2	147[d]	3.8	125[d]	4.6	120[d]	3.0	120[d]
1393.755	Si IV(1)	92.4	174	125.0	360[f]	33.7	99	27.5	93	27.5	103	87.9	204	69.4	203	—	—[h]	—	—[h]	—	—[h]
1399.774	O IV	—	—[e]	—	—	—	—[e]	—	—[e]	—	—[e]	—	—[e]	—	—	—	—[e]	1.7	140[c]	—	—[e]
1401.156	O IV	11.8	173	8.7	143	9.5	123[d]	11.3	147	6.2	125[d]	20.5	163	20.2	151	15.6	125	22.0	140	13.4	120
1402.770	Si IV(1)	52.0	183	65.0	340[f]	19.7	102	16.7	103	16.5	110	48.3	179	42.1	186	52.3	110	—	—[h]	46.1	125
1404.790[b]	O IV, S IV	5.2	164[d]	—	—[e]	—	—[e]	—	—[g]	—	—[e]	11.2	160[d]	12.7	157	7.0	125[d]	5.1	140[d]	6.6	115[d]

1406.000	S IV	—	—[e]	—	—[e]	—	—[e]	—	—[e]	—	—[e]	—	—[e]	—	—[e]	—	—[e]	—	—[g]	—	—[e]
1445.750[k]	Si VIII	—	—[e]	—	—[e]	—	—[e]	—	—[e]	—	—[e]	—	—[e]	—	—[e]	—	—[e]	—	—[g]	—	—[e]
1446.410	Unident.	—	—[e]	—	—[e]	—	—[e]	—	—[e]	—	—[e]	—	—[e]	—	—[e]	—	—[e]	—	—[g]	—	—[e]
1486.496	N IV(0.01)	7.2	161	—	—	—	—[e]	6.0	120	—	—[e]	15.2	161[d]	14.0	150	10.3	125	9.4	140	8.3	120
1526.708	Si II(2)	43.3	131	33.1	122	25.7	86	21.1	87	15.1	82	24.9	84	21.5	94	17.8	90	15.9	90	20.0	90
1533.432	Si II(2)	54.5	121	41.8	138	27.7	86	22.3	78	17.5	87	29.8	86	24.2	106	23.9	110	21.3	105	22.2	100
1548.185	C IV(1)	—	—[h]	336.0	230[f]	160.0	152	131.2	175	76.9	174	207.6	198	152.5	240	—	—[h]	—	—[h]	—	—[h]
1550.774	C IV(1)	129.7	290	162.0	260[f]	91.1	145	69.7	142	43.4	153	136.6	198	105.5	220	—	—[h]	—	—[h]	—	—[h]
1559.084	Fe II(45)	26.7	136	23.8	102	17.8	70	13.7	75	9.8	68	14.2	68	14.1	82	10.3	75	8.4	95	13.0	70
1560.290[b]	Fe II(45), C I	18.7	120	15.3	115	19.9	95	17.4	91	8.2	96[d]	20.0	96	18.6	92	5.0	95	—	—[g]	7.0	100
1560.689[b]	C I(3)	28.0	130	22.8	114	26.6	95	22.9	99	12.1	83	26.8	96	21.3	90	11.7	100	4.7	95	11.2	80
1561.423[b]	C I(3)	47.3	191	41.6	180	46.4	170	42.4	160	12.3	84	46.0	173	39.7	171	15.1	110	7.7	105	13.5	90
1563.788	Fe II(45)	25.5	115	21.4	95	18.0	68	14.2	61	9.2	65	15.4	70	12.9	71	11.8	92	7.5	95	13.6	70
1566.819	Fe II(44)	15.9	98	14.0	85	13.5	65	11.3	61	7.0	65[d]	11.3	62	10.4	71	7.7	95	4.3	90	8.2	70
1569.674	Fe II(44)	8.4	98	6.4	75[d]	9.3	67	7.6	61	4.5	74[d]	7.0	59[d]	7.4	65	3.5	90	1.5	—[i]	4.2	70
1570.242	Fe II(45)	17.1	117	15.2	86	14.9	66	11.4	55	7.2	69	12.4	67	11.2	69	8.0	90	4.6	95	8.9	65
1574.923	Fe II(45)	16.1	112	13.9	89	11.7	56	11.2	68	5.2	70[c]	11.5	67	9.7	56	6.3	90	3.6	95	7.8	65
1580.625	Fe II(44)	15.4	105	12.5	87	13.8	71	10.7	58	6.9	72[d]	12.0	70	10.7	70	6.0	85	3.7	95	7.1	65
1584.949	Fe II(44)	13.2	100	11.6	87	13.0	60	10.7	61	5.8	65[d]	10.1	60[d]	9.5	74	5.3	85	3.4	90	6.2	67
1588.286	Fe II(44)	10.0	110	6.7	82[d]	9.3	62	8.1	56	5.0	71[d]	8.7	62[d]	8.2	63	3.0	80	1.5	—[j]	3.9	70
1608.438	Fe II(8)	24.4	131	20.6	93	20.0	75	16.0	70	9.8	71	17.9	71	15.4	70	8.5	90	6.2	95	10.8	70
1610.921	Fe II(43)	13.1	117	9.6	80[d]	10.8	63	9.6	63	3.9	70[c]	9.4	65[d]	9.0	64	4.4	90	2.6	—[i]	4.7	65
1612.802	Fe II(43)	25.3	135	22.5	103	18.6	71	14.3	65	9.5	68	15.2	75	14.2	76	11.0	90	9.3	90	12.9	70
1618.470	Fe II(8)	12.4	95	11.4	91	14.4	69	12.0	64	5.2	68[d]	12.7	67	10.9	70	3.0	—[j]	—	—[e]	4.5	70
1621.685	Fe II(8)	9.2	101	8.6	107[d]	11.9	68[d]	9.6	65	4.2	70[c]	10.7	71[d]	9.2	66	3.4	95[c]	—	—[e]	3.7	70
1623.091	Fe II(8)	9.8	104	8.3	82[d]	10.0	61[d]	8.5	63	3.5	70[c]	9.1	67[d]	8.4	65	3.2	—[j]	—	—[e]	4.8	75
1625.520	Fe II(43)	24.2	129	20.1	94	18.5	70	14.2	61	8.5	65	13.2	65[d]	13.0	68	9.4	90	5.7	95	11.3	67
1633.908	Fe II(43)	18.7	118	15.5	91	17.9	75	12.8	70	6.6	66[d]	13.0	65	13.2	72	8.5	100	4.0	95	8.6	67
1637.397	Fe II(43)	23.4	128	18.3	87	18.1	65	15.3	63	8.8	67	15.0	64	13.1	64	9.0	95	5.7	100	11.3	67
1640.400[b]	He II, Fe II	—	—[h]	241.0	—	129.0	—[f]	97.0	—[f]	52.0	—[f]	116.0	—[f]	—	—[f]	—	—[h]	103.8	275[f]	128.0	265[f]

Wavelength[a] Å	Identification	P37 – Dec. 1, 1973						P39 – Dec. 5, 1973								P76 – Jan. 12, 1974					
		3B-006-8		3B-007-2		3B-024-7		3B-025-1		3B-025-2		3B-025-4		3B-025-5		3B-163-2		3B-163-6		3B-164-5	
		I	FWHM (mÅ)	I	FWHM (mÅ)	I	FWHM (mÅ)	I	FWHM (mÅ)	I	FWHM (mÅ)	I	FWHM (mÅ)	I	FWHM (mÅ)	I	FWHM (mÅ)	I	FWHM (mÅ)	I	FWHM (mÅ)
1643.576	Fe II(42)	19.5	110	15.3	75	17.9	65	15.0	66	7.6	65[d]	15.2	65	13.7	68	7.3	95	3.6	—[i]	7.8	65
1649.423	Fe II(42)	10.0	95	9.1	101[d]	12.5	68[d]	10.3	68	4.8	70[c]	11.0	69[d]	9.6	62	3.3	—[j]	—	—[e]	4.8	70
1656.267	C I(2)	47.5	107	36.9	110	39.4	90	29.1	93	15.0	83	37.6	93	31.3	93	12.2	100	6.8	95	14.2	70
1656.991[b]	C I(2)	93.8	171	81.3	188	56.5	160	65.0	167	38.6	150	71.9	167	61.7	173	38.3	150	22.6	125	41.1	140
1657.380	C I(2)	39.8	105	31.3	97	36.0	83	28.4	86	13.3	80	31.6	76	27.5	81	9.2	90	5.0	100	11.0	65
1657.907	C I(2)	35.0	106[c]	39.7	108	24.0	70	24.6	90	16.3	101	29.3	90[c]	27.2	85	11.9	95	6.7	95	13.9	70
1658.122	C I(2)	38.3	106[c]	42.5	104	34.0	74	30.6	86	17.6	102	33.6	91	28.2	85	13.5	90	7.9	100	15.5	65
1658.771	Fe II(41)	16.9	100	14.0	80	17.4	73	12.8	68	8.6	75[c]	17.4	90[c]	12.7	67	6.5	95	3.5	—[j]	8.2	70
1659.483	Fe II(40)	38.1	114	33.7	97	27.5	66	20.5	64	17.0	85	24.0	90[c]	19.1	63	14.8	90	11.1	95	17.4	65
1660.803	O III	—	—[e]	—	—[e]	—	—[e]	—	—[e]	—	—[e]	—	—[g]	8.9	133	4.6	140[c]	8.2	150	6.1	112
1663.221	Fe II(40)	—	—[e]	—	—[e]	7.9	75	12.0	68	6.4	66	14.6	79	11.5	64	5.8	90	2.9	—[j]	7.0	70
1666.153	O III	8.8	170	—	—[e]	—	—[e]	—	—[g]	—	—[e]	17.7	152[d]	21.8	172	16.3	140	24.7	150	18.1	100
1670.770[b]	Al II, Fe II	142.9	191	164.0	205[f]	77.5	114	62.4	124	53.4	114	85.2	134	73.7	134	79.6	130	80.0	150	71.3	140
1674.254	Fe II(41)	8.5	101	6.8	66[d]	11.3	78[d]	9.0	66[d]	—	—[e]	9.4	60[d]	8.8	62	2.8	—[j]	—	—[e]	3.7	70
1674.716	Fe II(40)	8.0	100	6.2	71[d]	10.7	71[d]	8.4	68[d]	—	—[e]	—	—[g]	8.6	74[d]	2.0	—[j]	—	—[e]	3.6	75
1685.954	Fe II(41)	8.9	108	8.2	99[d]	11.3	71[d]	9.0	66[d]	—	—[e]	10.0	67[d]	10.5	69	2.5	—[j]	—	—[e]	3.9	70
1686.455	Fe II(40)	11.2	100	8.8	80[d]	13.2	76[d]	10.1	61[d]	6.0	62[d]	11.4	69[d]	10.6	68	2.8	—[j]	—	—[e]	4.0	75
1686.692	Fe II(39)	12.0	100	—	—[e]	13.2	80[d]	10.0	64[d]	—	—[e]	8.9	57[d]	8.7	68[c]	2.9	—[j]	2.3	—[j]	4.6	75
1691.271	Fe II(41)	8.5	109	—	—[e]	10.4	80[d]	9.0	70[d]	—	—[e]	—	—[g]	8.6	64[d]	2.0	—[j]	—	—[e]	3.2	75[c]
1696.794	Fe II(38)	20.9	102	17.5	75	22.5	66	17.1	67	9.0	64[d]	20.1	66	18.2	66	7.6	90	3.7	—[j]	9.6	65
1702.043	Fe II(38)	69.8	162	63.1	107	42.4	77	33.3	63	24.4	80	36.7	79	32.8	82	28.9	90	25.4	95	38.2	70
1708.621	Fe II(38)	20.9	110	16.6	76	17.8	71	14.5	69	—	—[g]	15.1	62[d]	14.4	72	6.0	90	3.2	—[j]	7.5	70
1709.598	Ni II(4)	23.6	142	16.7	99	19.3	90	16.5	86	—	—[g]	18.1	95	19.2	103	6.0	115	2.9	—[j]	6.8	80
1712.997	Fe II(38)	65.8	119	56.3	95	43.7	72	34.6	60	23.2	72	39.5	71	34.5	71	27.6	90	19.1	90	31.1	70
1716.577	Fe II(39)	14.9	112	—	—[e]	13.0	77[d]	11.3	71[d]	—	—[e]	12.0	71	12.4	77	3.7	—[j]	—	—[e]	5.2	75

1720.616	Fe II(38)	45.0	118	40.8	104	31.5	79	23.8	70	14.5	70	25.1	76	26.2	71	18.3	90	12.7	95	21.0	75
1724.854	Fe II(39)	36.7	185	23.7	93	20.8	80	15.6	68	7.4	66[d]	19.0	73	18.0	72	10.9	120	4.6	—[j]	10.1	70
1726.391	Fe II(38)	34.7	119	30.6	95	28.1	78	21.6	71	12.0	72[d]	—	—[e]	20.2	69	13.0	95	6.5	90	14.9	70
1741.547	Ni II(5)	33.8	131	27.3	92	25.8	76	21.2	76	10.3	74[d]	21.6	71	23.2	82	10.7	100	5.0	—[j]	11.3	70
1748.285	Ni II(5)	21.0	113	20.3	115	22.7	77	17.6	71	9.4	83[d]	20.4	76[d]	17.7	77	6.3	90	3.4	—[j]	7.3	70
1749.600	Unident.	—	—[e]	—	—[e]	—	—[e]	—	—[e]	—	—[e]	—	—[e]	—	—[g]	—	—[g]	—	—[e]	—	—[g]
1751.911	Ni II(4)	25.9	107	19.8	91	22.5	83	17.9	77	8.2	70[d]	18.9	70[d]	—	—[g]	6.6	90	3.7	—[j]	8.9	80
1808.012	Si II(1)	164.0	120	159.1	103	120.0	81	90.0	69	41.1	84	120.9	75	97.5	83	55.1	90	56.0	110	64.6	80
1816.928	Si II(1)	—	—[h]	270.0	123	202.4	84	132.0	91	65.8	83	185.9	85	125.9	84	91.5	90	78.9	100	—	—[h]
1817.451	Si II(1)	20.5	93	23.0	84	29.0	80	24.7	79	7.7	61	36.7	71	32.3	70	6.2	90	4.9	100[c]	9.1	80
1854.716	Al III(1)	21.6	155	—	—[e]	—	—[e]	—	—[e]	—	—[e]	19.7	80	28.9	118	18.9	135	28.6	135	24.6	90
1862.790	Al III(1)	10.3	164	—	—[e]	—	—[e]	—	—[e]	—	—[e]	—	—[e]	14.4	102[d]	7.8	135[c]	11.0	135[c]	9.3	85
1892.030	Si III(1)	151.9	306	178.5	350[f]	51.8	107	38.0	108	46.8	109	137.0	214	133.4	228	141.7	160	236.5	190	152.8	125
1908.734	C III(0.01)	66.8	245	53.3	206[f]	49.9	137	34.0	124	30.4	139[d]	80.6	161	91.5	202	92.8	170	146.7	200	73.5	120
1930.905	C I(33)	119.4	147	117.0	117	101.0	100	82.0	90	40.0	86	99.0	97	81.3	98	41.4	100	19.3	115	36.9	85

[a] Wavelengths from Kelly and Palumbo (1973), except for blends and unidentified lines.
[b] Blend of two lines.
[c] Line width estimated from other lines of the same ion.
[d] Measured line width not reliable, line is too weak.
[e] Line absent.
[f] Line strongly asymmetric.
[g] Line present, but too weak for good measurement of both peak intensity and line width.
[h] Image of line overexposed on film.
[j] Intensity derived for assumed FWHM = 0.095 Å.
[k] Wavelength from Sandlin *et al.* (1977).

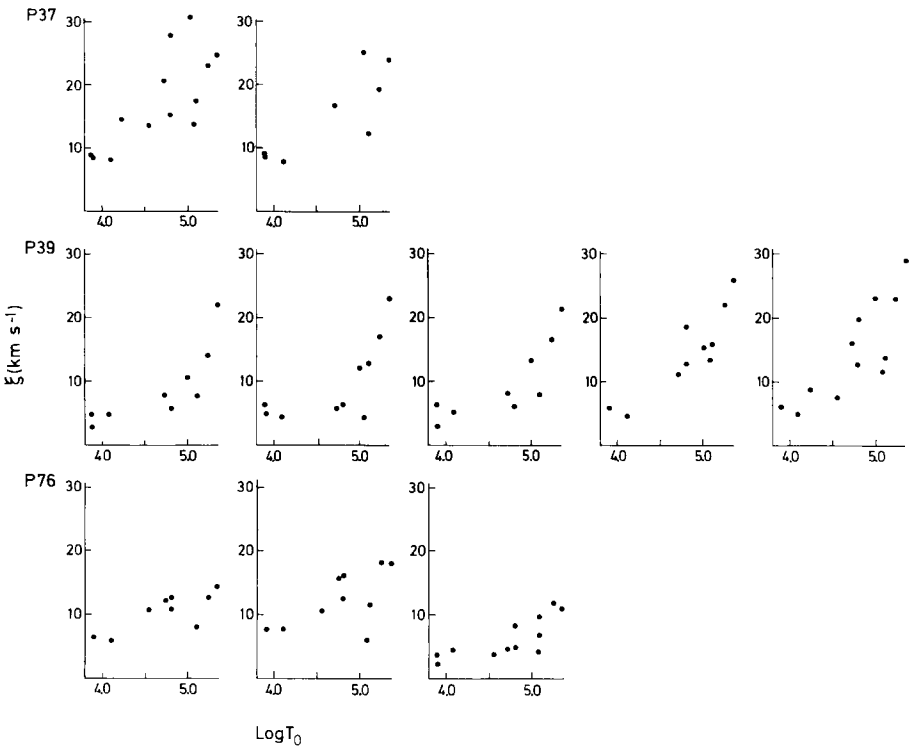

Fig. 2. The dependence of nonthermal velocities, ξ, on ion temperature, in prominences.

3.3. NONTHERMAL LINE BROADENING

We have noted that the observed profiles of the prominence lines are, with few exceptions, gaussian. If we assume that all line broadening mechanisms are also gaussian, the FWHM of an optically thin line can be written as

$$\mathrm{FWHM} = \left[W_I^2 + 4 \ln 2 \left(\frac{\lambda}{c}\right)^2 \left(\frac{2kT_i}{M_i} + \xi^2\right)\right]^{1/2};$$

W_I is the instrumental width, T_i the ion temperature, M_i the ion mass, and ξ the most probable speed corresponding to the nonthermal broadening.

In deriving the nonthermal broadening we assume the ion temperature equal to the electron temperature, and use the value, T_0, of the temperature corresponding to maximum ionization fraction at equilibrium for the ion species considered. T_0 is derived from the ionization equilibria of Jordan (1969) using the set of calculations including density effects in a solar model. For the instrumental width we use the value 0.06 Å.

It is important to restrict the analysis to optically thin lines, Mariska *et al.* (1978) have demonstrated that the use of intersystem lines alone lead to much better correlation of ξ vs T_0 than if both allowed and forbidden lines are used together. This

is because of optical depth effects occurring in the allowed resonance lines leading to broadening of these lines in excess of their absorption or emission profile widths.

In the prominence material we do not have a sufficiently large number of intersystem lines to allow reliable determination of the nonthermal broadening over the entire temperature range covered by the observations. But many of the allowed lines appear optically thin giving values for ξ which are not systematically different from those obtained from the intersystem lines. It should be mentioned, however, that the C IV lines at 1550 Å and the O V line at 1218.36 Å give particularly high nonthermal widths in prominences P37 and P39, respectively.

Results of the determination of the nonthermal widths are given in Figure 2, where ξ in km s^{-1} is plotted against log T_0. There is a clear connection between nonthermal width and gas temperature. Figure 2 suggests a nearly linear relationship between ξ and log T_0. The measured points scatter around linear regression lines with rms-values ranging from 5 km s^{-1} for P37 to 1 km s^{-1} for P76. Figure 2 also demonstrates the definite differences in nonthermal velocities between prominences. P37 has velocities not much different from those occurring in the quiet Sun or active regions. On the other hand P76 is very quiescent with nonthermal velocities hardly exceeding 10 km s^{-1} for exposure 3B-164-5.

The nonthermal broadening parameter is often interpreted as the most probable speed of turbulent random mass motions. These mass motions may be caused by the passage of acoustic or MHD waves through the gas and the variation of the non-thermal velocities with temperature related to the energy flux of the waves (Mariska *et al.*, 1978). However, with our lack of spatial resolution along a 60 arc sec long slit one can not exclude the possibility of the nonthermal broadening being caused by a large number of gas elements moving in a fashion which cannot be characterized as random motion. According to Engvold (1976) and Maltby (1976) large scale mass motions with velocities of a few km s^{-1} appear to be common in quiescent prominences. Also smaller regions with high average velocities of 30 km s^{-1} are present (Engvold and Malville, 1977).

3.4 Electron Pressure and Density

In recent years calculations have been made giving the density dependence for a number of density sensitive line ratios in the spectral range 1175 Å to 1930 Å. A particular line ratio is not applicable to all types of solar features. An important condition is that the observed intensity ratio should fall in a range where it is most sensitive to variations in density. The intensity ratio must be as independent of temperature as possible, otherwise the result will depend too heavily on the assigned temperature of formation. Also the lines must be optically thin.

It is preferable that both lines compared come from the same ion. This eliminates errors caused by uncertain element abundances. Only few lines of this type are available in the prominence material. Examples are the ratio of the C III multiplet at 1176 Å to the intersystem line at 1908.73 Å. Another possibility is the O IV ratio, $I(1404.79/I(1401.15)$.

For reasons described below none of these ratios appear to be ideal for density measurements in prominences. We have therefore relied on the following ratios: I(Si III 1892)/I(C III 1909), I(Si IV 1403)/I(C III 1909), and I(C III 1909)/I(O III 1666). Data for the first two ratios are taken from the calculations of Cook and Nicolas (1978). For the ratio R(1403/1909) the calculations for an isothermal gas was used to determine the electron density, N_e, and an estimated average temperature of formation for the two lines was set at 67 000 K. For the ratio R(1892/1909) the pressure scale given by Cook and Nicolas for integration through an atmosphere model were used. The ratio R(1909/1666) is taken from Doschek *et al.* (1978) and a temperature of formation of 60 000 K was assigned to find the electron pressure.

The results are presented in Table III. The derived pressures (in dyn cm^{-2}) are in agreement within the accuracy of the pressure determination. The average pressure determined from the values listed in Table III are 0.14 ± 06 dyn cm^{-2} for P37, 0.05 ± 0.02 dyn cm^{-2} for P39 and 0.06 ± 0.02 dyn cm^{-2} for P76. The values given as uncertainties only reflect the scatter in the data, the actual uncertainties probably being larger.

The very low pressure derived from the ratio R(1909/1666) for exposure 3B-006-8 is most likely caused by the low intensity of the O III line. The measured intensity of this line becomes very uncertain. Raising the intensity of the O III line by a factor 1.5–2.0 would bring the pressure determined from this ratio into agreement with the other pressures measured for P37.

Table III also includes results from the C III line ratio R(1176/1909) suggesting low pressure values. The theoretical calculations are again taken from Cook and

TABLE III

Electron pressures in dyn cm^{-2} from density sensitive line ratios

Prominence and plate-identification	Line pairs and temperatures of formation			
	R(1892/1909)	R(1405/1909)	R(1909/1666)	R(1176/1909)[b]
	56 000 K	67 000 K	60 000 K	56 000 K
3B-006-8	0.075	0.123	0.025[a]	0.008
3B-007-2	0.125	0.220	—	0.011
3B-024-7	0.026	0.043	—	—
3B-025-1	0.029	0.061	—	0.020
3B-025-2	0.044	0.072	—	—
3B-025-4	0.041	0.055	0.076	0.015
3B-025-5	0.051	0.074	0.067	0.012
3B-163-2	0.047	—	0.039	—
3B-163-6	0.044	0.076	0.043	—
3B-164-5	0.067	0.090	0.082	—

[a] λ 1666 very faint.

[b] Using total intensity $I(1176) \approx 2.3 \times I(1175.71)$.

Nicolas (1978). This deviation is not just occurring in prominences. Generally, pressures determined from $R(1176/1909)$ fall below pressures determined from $R(1892/1909)$ and $R(1403/1909)$ by factors of six (Cook and Nicolas, 1978). The reason for this is not completely clear, but it is difficult to reconcile the difference with errors in the relative abundance of silicon to carbon. Cook and Nicolas discuss various other possibilities and conclude that optical density effects in the 1176 Å line are the most likely explanation. For this reason, and also because the measured ratios are close to the low density saturation value, we regard the ratio $R(1176/1909)$ as unreliable for determining the electron pressure.

The O IV ratio, $R(1405/1401)$, is also unsuitable. Both lines are weak in prominences and the 1404.79 Å line is blended with a S IV line. In our prominence material no other lines of the same S IV multiplet are measurable. Thus it is not possible to subtract out the contribution of the S IV line to the blend at 1404.77 Å. Using the uncorrected intensity of the blend will only lead to lower limits for the densities and pressures.

4. Comparison with Other Investigations

It is difficult to compare our measured prominence intensities with those reported by Noyes *et al.* (1972), Schmahl *et al.* (1974) and Orrall and Schmahl (1976). These authors give the prominence intensities relative to the quiet Sun, and in the case of Orrall and Schmahl the quiet Sun values specifically represent the center of a network cell.

The comparison is complicated by the different ways intensities are averaged over prominence and quiet Sun fine structures by the different instruments. An attempt has been made to compare S082B intensity ratios of prominences to the quiet Sun with the values of Orrall and Schmahl for the few lines common to both investigations. As quiet Sun intensities for S082B we used the disc intensity values given in a solar spectral atlas by Kjeldseth Moe *et al.* (1976). The atlas spectra were derived from an S082B CALROC flight. Taking into account the probable contribution from network boundaries to the atlas intensities and using the fill factors of Table I the agreement with Orrall and Schmahl (1976) is satisfactory considering the errors of calibration. The comparison can only be approximate since the actual network contribution to the atlas intensity is unknown.

Comparison with the work of Yang *et al.* (1975) shows systematic variations with wavelength. The ratio of the average prominence intensities reported by Yang *et al.* to our values varies from ≈ 2.0 for wavelengths below 1240 Å to 0.7 at 1394 Å on the average. As pointed out by Schmahl (1978), these systematic variations may be caused by a calibration error by Yang *et al.* (1975).

Our value for the electron pressure, ≈ 0.05 dyn cm^{-2} for P39 and P76 and ≈ 0.1 dyn cm^{-2} for P37, differ from the values of other investigations. Noyes *et al.* (1972), Orrall and Speer (1974), Schmahl *et al.* (1974), and Orrall and Schmahl (1976) all report pressures in the range 0.01 to 0.02 dyn cm^{-2}. These investigations

all use the density sensitive lines of C III at 977 Å and 1176 Å. It should be pointed out that our data give pressures in the same range when the ratio $R(1176/1909)$ is used. The discussion of Cook and Nicolas (1978) covers possible errors in the S082B calibration, optical density effects in the 1176 Å line and dynamical equilibrium effects. S082B appear to be well calibrated down to Lα at 1216 Å. Calibration errors below this wavelength may possibly raise the intensity of 1176 Å by a factor 1.5–2.0 leading to higher electron pressure values from the ratio $R(1176/1909)$. While this would improve the consistency between values in Table III it does nothing to explain the difference between the S082B measurements and other investigations. For this the possibility of optical density effects in the 1176 Å line appear more promising. However, it remains to do a quantitative estimate demonstrating this argument.

Acknowledgements

This work was supported by NASA under DPR S60404G, and by the Norwegian Foundation for Science and the Humanities.

References

Bartoe, J. -D. F., Brueckner, G. E., Purcell, J. D., and Tousey, R.: 1977, *Appl. Opt.* **16**, 879.
Cook, J. W. and Nicolas, K. R.: 1978, *Bull. Am. Astron. Soc.* **10**, 439.
Doschek, G. A., Feldman, U., Bhatia, A. K., and Mason, H. E.: 1978; *Astrophys. J.* **226**, 1129.
Engvold, O.: 1976, *Solar Phys.* **49**, 283.
Engvold, O. and Malville, J. McKim: 1977, *Solar Phys.* **52**, 369.
Feldman, U. and Doschek, G.: 1977, *Astrophys. J. Letters* **216**, L119.
Flower, D. R. and Nussbaumer, H.: 1975, *Astron. Astrophys.* **45**, 145.
Jordan, C.: 1969, *Monthly Notices Roy. Astron. Soc.* **142**, 501.
Kelly, R. L. and Palumbo, L.: 1973, NRL Report 7599, Naval Research Laboratory, Washington D.C.
Kjeldseth Moe, O. and Nicolas, K. R.: 1977, *Astrophys. J.* **211**, 579.
Kjeldseth, Moe, O. and Milone, E. F.: 1978 *Astrophys. J.* **226**, 301.
Kjeldseth Moe, O., VanHoosier, M. E., Bartoe, J.-D. F., and Brueckner, G. E.: 1976, *A Spectral Atlas of the Sun Between 1175 and 2100 Ångstroms*, NRL Report 8057, Naval Research Laboratory, Washington, D.C.
Maltby, P.: 1976, *Solar Phys.* **46**, 149.
Mariska, J. T., Feldman, U., and Doschek, G. A.: 1978, *Astrophys. J.* **226**, 698.
Markey, J. F. and Austin, R. R.: 1977, *Appl. Opt.* **16**, 917.
Noyes, R., Dupree, A., Huber, M., Parkinson, W., Reeves, E., and Withbroe, G.: 1972, *Astrophys. J.* **178**, 515.
Orrall, F. and Schmahl, E.: 1976, *Solar Phys.* **50**, 365.
Orrall, F. and Speer, R.: 1974, in R. G. Athay (ed.) 'Chromospheric Fire Structures', *IAU Symp.* **56**, 193.
Sandlin, G. D., Brueckner, G. E., and Tousey, R.: 1977, *Astrophys. J.* **214**, 898.
Schmahl, E.: 1978, in Jensen, Maltby, and Orrall (eds.), 'Physics of Solar Prominences', *IAU Colloq.* **44**, 102.
Schmahl, E., Foukal, P., Huber, M., Noyes, R., Reeves, E., Timothy, J. G., Vernazza, J., and Withbroe, G.: 1974, *Solar Phys.* **39**, 337.
Speer, R., Garton, W., Goldberg, L., Parkinson, W., Reeves, E., Morgan, A., Nicholls, R., James, T., Paxton, J., Shenton, D., and Wilson, R.: 1970, *Nature* **226**, 249.
VanHoosier, M. E.: 1978, private communication.
Withbroe, G.: 1971, *Solar Phys.* **18**, 458.
Yang, C., Nicholls, R., and Morgan, F.: 1975, *Solar Phys.* **45**, 351.